Predicting the Sequence-Dependent Backbone Dynamics of Intrinsically Disordered Proteins

Sanbo Qin[1] and Huan-Xiang Zhou[1,2,*]

[1]Department of Chemistry and [2]Department of Physics, University of Illinois at Chicago, Chicago, IL 60607, USA

*Corresponding author. E-mail: hzhou43@uic.edu

Abstract

Dynamics is a crucial link between sequence and function for intrinsically disordered proteins (IDPs). NMR spin relaxation is a powerful technique for characterizing the sequence-dependent backbone dynamics of IDPs. Of particular interest is the ^{15}N transverse relaxation rate (R_2), which reports on slower dynamics (10s of ns up to 1 μs and beyond). NMR and molecular dynamics (MD) simulations have shown that local interactions and secondary structure formation slow down backbone dynamics and raise R_2. Elevated R_2 has been suggested to be indicators of propensities of membrane association, liquid-liquid phase separation, and other functional processes. Here we present a sequence-based method, SeqDYN, for predicting R_2 of IDPs. The R_2 value of a residue is expressed as the product of contributing factors from all residues, which attenuate with increasing sequence distance from the central residue. The mathematical model has 21 parameters, representing the correlation length (where the attenuation is at 50%) and the amplitudes of the contributing factors of the 20 types of amino acids. Training on a set of 45 IDPs reveals a correlation length of 5.6 residues, aromatic and long branched aliphatic amino acids and Arg as R_2 promotors whereas Gly and short polar amino acids as R_2 suppressors. The prediction accuracy of SeqDYN is competitive against that of recent MD simulations using IDP-specific force fields. For a structured protein, SeqDYN prediction represents R_2 in the unfolded state. SeqDYN is available as a web server at https://zhougroup-uic.github.io/SeqDYNidp/ for rapid R_2 prediction.

Keywords: intrinsically disordered proteins; NMR spin relaxation; transverse relaxation rate; backbone dynamics; R_2 prediction

Significance Statement

How the sequences of intrinsically disordered proteins (IDPs) code for functions is still an enigma. Dynamics, in particular residue-specific dynamics, holds crucial clues. Enormous efforts have been spent to characterize residue-specific dynamics of IDPs, mainly through NMR spin relaxation experiments. Here we present a sequence-based method, SeqDYN, for predicting residue-specific backbone dynamics of IDPs. SeqDYN employs a mathematical model with 21 parameters and is trained on 45 IDPs. It provides not only rapid, accurate prediction but also insightful physical interpretation of sequence-dependent IDP dynamics.

Introduction

Intrinsically disordered proteins (IDPs) or regions (IDRs) do not have the luxury of a three-dimensional structure to help decipher the relationship between sequence and function. Instead, dynamics has emerged as a crucial link between sequence and function for IDPs (1). NMR spin relaxation is a uniquely powerful technique for characterizing IDP dynamics, capable of yielding residue-specific information (2). Backbone ^{15}N relaxation experiments typically yield three parameters per residue: transverse relaxation rate (R_2), longitudinal relaxation rate (R_1), and steady-state heteronuclear Overhauser enhancement (NOE). While all the three parameters depend on ps-ns dynamics, R_2 is the one most affected by slower dynamics (10s of ns to 1 μs and beyond). An increase in either the timescale or the amplitude of slower dynamics results in higher R_2. For IDPs, R_2 is also the parameter that exhibits the strongest dependence on sequence (1, 2).

R_2 was noted early on as an important indicator of residual structure in the unfolded state of the structured protein lysozyme (3). This property has since been measured for many IDPs to provide insight into various biophysical processes. Just as the residual structure in the unfolded state biases the folding pathway of lysozyme (3), a nascent α-helix in the free state of Sendai virus nucleoprotein C-terminal domain (Sev-NT), as indicated by highly elevated R_2 (4), biases the coupled binding and folding pathway in the presence of its target phosphoprotein (5). Local secondary structure preformation also facilitates the binding of yes-associated protein (YAP) with its target transcription factor (6). Likewise a correlation has been found between R_2 in the free state and the membrane binding propensity of synaptobrevin-2: residues with elevated R_2 have increased propensity for membrane binding (7). R_2 in the free state has also been used to uncover factors that promote liquid-liquid phase separation of IDPs. For example, a nascent α-helix (shown by elevated R_2) is important for the phase separation of TDP-43 low-complexity domain, as both the deletion of the helical region and a helix-breaking mutation (Ala to Pro) abrogates phase separation (8). Similarly, nascent α-helices in the free state of cytosolic abundant heat-soluble 8 (CAHS-8), upon

raising concentration and lowering temperature stabilize to form the core of fibrous gels (9). For hnRNPA1 low-complexity domain (A1-LCD), aromatic residues giving rise to local peaks in R_2 also mediate phase separation (10).

Both NMR relaxation data and molecular dynamics (MD) simulations have revealed determinants of R_2 for IDPs. It has been noted that the flexible Gly has a tendency to lower R_2 whereas secondary structure and contact formation tend to raise R_2 (11). This conclusion agrees well with recent MD simulations (1, 12-14). These MD studies, using IDP-specific force fields, are able to predict R_2 in quantitative agreement with NMR measurements, without ad hoc reweighting as done in earlier studies. According to MD, most contact clusters are formed by local sequences, within blocks of up to a dozen or so residues (1, 12, 13). Tertiary contacts can also form but are relatively rare; as such their accurate capture requires extremely extensive sampling and still poses a challenge for MD simulations. Opposite to Gly, aromatic residues have been noted as mediators of contact clusters (3, 10).

Schwalbe et al. (15) introduced a mathematical model to describe the R_2 profile along the sequence for lysozyme in the unfolded state. The R_2 value of a given residue was expressed as the sum of contributions from this residues and its neighbors. This model yields a mostly flat profile across the sequence, except for falloff at the termini, resulting an overall bell shape. Klein-Seetharaman et al. (3) then fit peaks above this flat profile as a sum of Gaussians. Cho et al. (16) proposed bulkiness as a qualitative indicator of backbone dynamics. Recently Sekiyama et al. (17) calculated R_2 as the geometric mean of "indices of local dynamics"; the latter were parameterized by fitting to the measured R_2 for a single IDP. All these models merely describe the R_2 profile of a given IDP, and none of them is predictive.

Here we present a method, SeqDYN, for predicting R_2 of IDPs. Using a mathematical model introduced by Li et al. (18) to predict propensities for binding nanoparticles and also adapted for predicting propensities for binding membranes (19), we express the R_2 value of a residue as the product of contributing factors from all residues. The contributing factor

attenuates as the neighboring residue becomes more distant from the central residue. The model, after training on a set of 45 IDPs, has prediction accuracy that is competitive against that of the recent MD simulations using IDP-specific force fields (1, 12-14). For lysozyme, the SeqDYN prediction agrees remarkably well with R_2 measured in the unfolded state.

Results

The data set of IDPs with R_2 rates

We collected R_2 data for a total of 54 nonhomologous IDPs or IDRs (Table S1; Fig. S1). According to indicators from NMR properties, including low or negative NOEs, narrow dispersion in backbone amide proton chemical shifts, and small secondary chemical shifts (SCSs), most of the proteins are disordered with at most transient α-helices. A few are partially folded, including Sev-NT with a well-populated (~80%) long helix (residues 478-491) (20), CREB-binding protein fourth intrinsically disordered linker (CBP-ID4) with > 50% propensities for two long helices (residues 2-25 and 101-128) (21), HOX transcription factor DFD (HOX-DFD) with a well-folded domain comprising three helices (22), and Hahellin (apo form) as a molten globule (23). In Fig. 1, we display representative conformations of five IDPs, ranging from fully disordered MAPK kinase 4 (MKK4) (24) and α-synuclein (25) to Measles virus phosphoprotein N-terminal domain (Mev-P_{NTD}) (26) with transient short helices to Sev-NT and CBP-ID4 with stable long helices. The sequences of all the IDPs are listed in Table S2.

We used 45 of the 54 IDPs to train and validate SeqDYN and reserved the remaining 9 for testing. The sequence lengths of the training set range from 39 to 406 residues, with an average of 125.3 residues. Altogether R_2 data are available for 3966 residues. A large majority (35 out of 45) of the 45 IDPs have mean R_2 values ($\bar{R}_2$, calculated among all the residues in a protein) between 2.5 and 5.5 s^{-1} (Table S1 and Fig. 2A). This $\bar{R}_2$ range is much lower than that of structured proteins with similar sequence lengths. The low $\bar{R}_2$ values and

lack of dependence on sequence length (Fig. S2A) suggest that R_2 of the IDPs is mostly dictated by local sequence as opposed to tertiary interaction.

The most often used temperature for acquiring the R_2 data was 298 K, but low temperatures (277 to 280 K) were used in a few cases (Table S1 and Fig. S2B). Of the seven IDPs with $\bar{R}_2 > 6.4$ s^{-1}, four can be attributed to low temperatures (27-30), one is due to a relatively low temperature (283 K) as well as the presence of glycerol (20% v/v) (31), and two can be explained by tertiary structure formation [a folded domain (22) or molten globule (23)]. A simple reason for higher R_2 values at lower temperatures is the higher water viscosity, resulting in slowdown in molecular tumbling; a similar effect is achieved by adding glycerol. In some cases, R_2 was measured at both low and room temperatures (4, 10). To a good approximation, the effect of lowering temperature is a uniform scaling of R_2 across the IDP sequence. For Sev-NT, downscaling of the R_2 values at 278 K by a factor of 2.0 brings them into close agreement with those at 298 K (Fig. S2C), with a root-mean-square-deviation (RMSD) of 0.5 s^{-1} among all the residues. Likewise, for A1-LCD, downscaling by a factor of 2.4 brings the R_2 values at 288 K into good match with those at 298 K (Fig. S2D), with an RMSD of 0.4 s^{-1}. Because SeqDYN is concerned with the sequence dependence of R_2, a uniform scaling has no effect on model parameter or prediction; therefore mixing the data from different temperatures is justified. The same can be said about the different magnetic fields in acquiring the R_2 data (Table S1 and Fig. S2E). Increasing the magnetic field raises R_2 values, and the effect is also approximated well by a uniform scaling (4, 8, 29).

One measure on the level of sequence dependence of R_2 is the standard deviation, σ_{R_2}, calculated among the residues of an IDP. Among the training set, the R_2 values of 30 IDPs have moderate sequence variations, with σ_{R_2} ranging from 0.5 to 1.5 s^{-1} (Table S1); the histogram of σ_{R_2} calculated for the entire training set peaks around 0.75 s^{-1} (Fig. 2A). There is a moderate correlation between σ_{R_2} and $\bar{R}_2$ (Fig. 2A, inset), reflecting in part the fact that σ_{R_2} can be raised simply by a uniform upscaling, e.g., as a result of lowering temperature. Still, only two of the five IDPs with high $\bar{R}_2$ attributable to lower temperature or presence of

glycerol are among the seven IDPs with high sequence variations ($\sigma_{R_2} > 2$ s^{-1}). Therefore the sequence variation of R_2 as captured by σ_{R_2} manifests mostly the intrinsic effect of the IDP sequence, not the influence of external factors such as temperature or magnetic field strength. The mean σ_{R_2} value among the training set is 1.24 s^{-1}.

One way to eliminate the influence of external factors is to scale the R_2 values of each IDP by its $\bar{R}_2$; we refer to the results as scaled R_2, or sR_2. We then pooled the sR_2 values for all residues in the training set, and separated them according to amino-acid types. The amino acid type-specific mean sR_2 values, or msR_2, are displayed in Fig. 2B. The seven amino acids with the highest msR_2 are, in descending order, Trp, Arg, Tyr, Phe, Ile, His, and Leu. The presence of all the four aromatic amino acids in this "high-end" group immediately suggests π-π stacking as important for raising R_2; the presence of Arg further implicates cation-π interactions. In the other extreme, the seven amino acids with the lowest msR_2 are, in ascending order, are Gly, Cys, Val, Asp, Ser, Thr, and Asn. Gly is well-known as a flexible residue; it is also interesting that all the four amino acids with short polar sidechains are found in this "low-end" group. Pro has an excessively low msR_2 [with data from only two IDPs (32, 33)], but that is due to the absence of an amide proton.

The SeqDYN model and parameters

The null model is to assume a uniform R_2 for all the residues in an IDP. The root-mean-square-error (RMSE) of the null model is equal to the standard deviation, σ_{R_2}, of the measured R_2 values. The mean RMSE, $\overline{\text{RMSE}}$, of the null model, equal to 1.24 s^{-1} for the training set, serves as the upper bound for evaluating the errors of R_2 predictors. The next improvement is a one-residue predictor, where first each residue (with index n) assumes its amino acid-specific mean sR_2 (msR_2) and then a uniform scaling factor Υ is applied:

$$R_2(n) = \Upsilon \cdot \text{ms}R_2(n) \quad (1)$$

This one-residue model does only minutely better than the null model, with a $\overline{\text{RMSE}}$ of 1.22 s^{-1}.

In SeqDYN, we account for the influence of neighboring residues. Specifically, each residue i contributes a factor $f(i;n)$ to the R_2 value of residue n. Therefore

$$R_2(n) = \Upsilon \prod_{i=1}^{N} f(i;n) \tag{2a}$$

where N is the total number of residues in the IDP. The contributing factor depends on the sequence distance $s = |i - n|$ and the amino-acid type of residue i:

$$f(i;n) = 1 + \frac{q(i) - 1}{1 + bs^2} \tag{2b}$$

There are 21 global parameters. The first 20 are the q values, one for each of the 20 types of amino acids; the last parameter is b, appearing in the Lorentzian form of the sequence-distance dependence. We define the correlation length, L_{corr}, as the sequence distance at which the contributing factor is midway between the values at $s = 0$ and ∞. It is easy to verify that $L_{\text{corr}} = b^{-1/2}$. Note that the single-residue model can be seen as a special case of SeqDYN, with L_{corr} set to 0 and q set to msR_2.

The functional forms of Eqs (2a,b) were adapted from Li et al. (18); we also used them for predicting residue-specific membrane association propensities of IDPs (19). In these previous applications, a linear term was also present in the denominator of Eq (2b). In our initial training of SeqDYN, the coefficient of the linear term always converged to near zero. We thus eliminated the linear term. In addition to the Lorentzian form, we also tested a Gaussian form for the sequence-distance dependence and found somewhat worse performance. The more gradual attenuation of the Lorentzian form with increasing sequence distance evidently provides an overall better model for the R_2 data in the entire training set. Others (16, 17, 24) have modeled R_2 as the average of some parameters over a window; a window has an extremely abrupt sequence-distance dependence (1 for $s < L_{\text{corr}}$ and 0 for $s > L_{\text{corr}}$).

We parametrized the SeqDYN model represented by Eqs (2a,b) on the training set of 45 IDPs. In addition to the 21 global parameters noted above, there are also 45 local parameters, namely one uniform scaling factor (ϒ) per IDP. The parameter values were selected to minimize the sum of the mean-square-errors for the IDPs in the training set, calculated on R_2 data for a total of 3924 residues. We excluded the 42 Pro residues in the training set because, as already noted, their R_2 values are lower for chemical reasons. We will present validation and test results below, but first let us look at the parameter values.

The q values are displayed in Fig. 2B alongside msR_2. The seven amino acids with the highest q values, in descending order, are Trp, Ile, Tyr, Arg, His, Phe, and Leu. These are exactly the same amino acids in the high-end group for msR_2, though their order there is somewhat different. The seven amino acids (excluding Pro) with the lowest q values, in ascending order, are Gly, Asn, Ser, Asp, Val, Thr, and Cys. The composition of the low-end group is also identical to that for msR_2. The q values thus also suggest that π-π and cation-π interactions in local sequences may raise R_2, whereas Gly and short-polar residues may lower R_2.

Given the common amino acids at both the high and low ends for msR_2 and q, it is not surprising that these two properties exhibit a strong correlation, with a coefficient of determination (R^2; excluding Pro) at 0.92 (Fig. 3A). Also, because the high-end group contains the largest amino acids (e.g., Trp and Tyr) whereas the low-end group contains the smallest amino acids (e.g., Gly and Ser), we anticipated some correlation of msR_2 and q with amino-acid size. We measure the latter property by the molecular mass (m). As shown in Fig. 3B, both msR_2 and q indeed show medium correlation with m, with $R^2 = 0.67$ (excluding Pro) and 0.61, respectively. A bulkiness parameter was proposed as an indicator of sequence-dependent backbone dynamics of IDPs (16, 24). Bulkiness was defined as the sidechain volume to length ratio, and identifies amino acids with aromatic or branched aliphatic sidechains as bulky (34). We found only modest correlations between either msR_2 or q and bulkiness, with R^2 just below 0.4 (Fig. 3C).

The optimized value of b is 3.164×10^{-2}, corresponding to an L_{corr} of 5.6 residues. The resulting optimized $\overline{\mathrm{RMSE}}$ is 0.95 s^{-1}, a clear improvement over the value 1.24 s^{-1} of the null model. To check the sensitivity of prediction accuracy to b, we set b to values corresponding to $L_{\mathrm{corr}} = 0, 1, 2, ..$, and retrained SeqDYN for b fixed at each value. Note that the null-model $\overline{\mathrm{RMSE}}$, 1.24 s^{-1}, sets an upper bound. This upper bound is gradually reached when L_{corr} is increased from the optimal value. In the opposite direction, when L_{corr} is decreased from the optimal value, $\overline{\mathrm{RMSE}}$ rises quickly, reaching 1.22 s^{-1} at $L_{\mathrm{corr}} = 0$. The latter $\overline{\mathrm{RMSE}}$ is the same as that of the single-residue model. Lastly we note that there is strong correlation between the uniform scaling factors and $\bar{R}_2$ values among the 45 IDPs ($R^2 = 0.77$), as to be expected. For 39 of the 45 IDPs, Υ values fall in the range of 0.8 to 2.0 s^{-1}.

As presented next, we evaluate the performance of SeqDYN by leave-one-out cross validation, where each IDP in turn was left out of the training set and the model was trained on the remaining 44 IDPs to predict R_2 for the IDP that was left out. The parameters from the leave-one-out (also known as jackknife) training sessions allow us to assess potential bias of the training set. For this purpose, we compare the values of the 21 global parameters, either from the full training set or from taking the averages of the jackknife training sessions. For each of the q parameters, the values from these two methods differ only in the fourth digit; e.g., for Leu, they are both 1.1447 from full training and from jackknife training. The values for b are 3.164×10^{-2} from full training as stated above and 3.163×10^{-2} from jackknife training. The close agreement in parameter values between full training and jackknife training suggests no significant bias in the training set.

Another question of interest is whether the difference between the q parameters of two amino acids is statistically significant. To answer this question, we carried out five-fold cross-validation training, resulting in five independent estimates for each parameter. For example, the mean ± standard deviation of the q parameter is 1.1405 ± 0.0066 for Leu and 1.2174 ± 0.0211 for Ile. A t-test shows that their difference is statistically significant ($P < 0.0001$). In contrast, the difference between Leu and Phe ($q = 1.1552 \pm 0.0304$) is not significant.

Validation of SeqDYN predictions

We now present leave-one-out cross-validation results. We denote the RMSE of the R_2 prediction for the left-out IDP as RMSE(-1). As expected, RMSE(-1) is higher than the RMSE obtained with the IDP kept in the training set, but the increases are generally slight. Specifically, all but eight of the IDPs have increases < 0.1 s^{-1}; the largest increase is 0.35 s^{-1}, for CBP-ID4. The mean RMSE(-1), or $\overline{\mathrm{RMSE}}(-1)$, for the 45 IDPs is increased by 0.05 s^{-1} over $\overline{\mathrm{RMSE}}$, to 1.00 s^{-1}. The latter value is still a distinct improvement over the mean RMSE 1.24 s^{-1} of the null model. The histogram of RMSE(-1) for the 45 IDPs is shown in Fig. 4A. It peaks at 0.5 s^{-1}, which is a substantial downshift from the corresponding peak at 0.75 s^{-1} for σ_{R_2} (Fig. 2A). Thirty-four of the 45 IDPs have RMSE(-1) values lower than the corresponding σ_{R_2}.

To further illustrate the performance of SeqDYN, we present comparison of predicted and measured R_2 values for five IDPs: MKK4, α-synuclein, Mev-P_{NTD}, Sev-NT, and CBP-ID4 (Fig. 4B-F). A simple common feature is the falloff of R_2 at the N- and C-termini, resulting from missing upstream or downstream residues that otherwise would be coupled to the terminal residues, as first recognized by Schwalbe et al. (15). Representative conformations of the five IDPs are displayed in Fig. 1, with residues colored according to the predicted R_2 values. For four of these IDPs, the RMSE(-1) values range from 0.44 to 0.76 s^{-1} and are scattered around the peak of the histogram, while the RMSE(-1) for the fifth IDP, namely CBP-ID4, the RMSE(-1) value is 2.01 s^{-1} and falls on the tail of the histogram (Fig. 4A). Figure 4B displays the measured and predicted R_2 for MKK4. SeqDYN correctly predicts higher R_2 values in the second half of the sequence than in the first half. It even correctly predicts the peak around residue Arg75. The sequence in this region is H_{72}IERLRTH_{79}; six of these eight residues belong to the high-end group. In contrast, the lowest R_2 values occur in the sequence S_7GGGGSGGGSGSG$_{19}$, comprising entirely of two amino acids in the low-end group.

R_2 values for α-synuclein are shown in Fig. 4C. Here SeqDYN correctly predicts higher R_2 near the C-terminus and a dip around Gly68. However, it misses the R_2 peaks around Tyr39 and Asp121. MD simulations (1) have found that these R_2 peaks can be explained by a combination of secondary structure formation (β-sheet around Tyr39 and polyproline II helix around Asp121) and local (between Tyr39 and Ser42) or long-range (between Asp121 and Lys96) interactions. SeqDYN cannot account for long-range interactions (e.g., between β-strands and between Asp121 and Lys96). Figure 4D shows that SeqDYN gives excellent R_2 predictions for Mev-P_{NTD}. It correctly predicts the high peaks around Arg17, Glu31, Leu193, and lower peaks around Arg235 and Trp285, but does underpredict the narrow peak around Tyr113.

The overall R_2 profile of Sev-NT is predicted well by SeqDYN, but the peak in the long helical region (residues 478-491) is severely underestimated (green curve in Fig. 4E). A similar situation occurs for CBP-ID4, where the peak in the second long helical region (around Glu113) is underpredicted (green curve in Fig. 4F). While the measured R_2 exhibits a higher peak in the second helical region than in the first helical region (around Arg16), the opposite is predicted by SeqDYN. When the R_2 data were included in the training set (i.e., full training), the second peak is higher than the first one, but that is not a real prediction because the R_2 data themselves were used for training the model. It merely means that the SeqDYN functions can be parameterized to produce any prescribed R_2 profile along the sequence. Indeed, when the R_2 data of CBP-ID4 alone were used to parameterize SeqDYN, the measured R_2 profile is closely reproduced (Fig. S3). The reversal in R_2 peak heights between the two helical regions is the reason for the aforementioned unusual increase in RMSE when CBP-ID4 was left out of the training set.

R2 boost in long helical regions

It is apparent that SeqDYN underestimates the R_2 of stable long helices. Transient short helices does not seem to be a problem, since these are present, e.g., in Mev-P_{NTD}, where

transient helix formation in the first 37 residues and between residues 189-198 (26) coincides with R_2 peaks that are correctly predicted by SeqDYN. SeqDYN can treat coupling between residues within the correlation length of 5.6 residues, but a much longer helix would tumble more slowly than implied by an L_{corr} of 5.6, and thus it makes sense that SeqDYN would underestimate R_2 in that case.

Our solution then is to apply a boost factor to the long helical region. To do so, we have to know whether an IDP does form long helices and if so what the constituent residues are. Secondary structure predictors tend to overpredict α-helices and β-strands for IDPs, as they are trained on structured proteins. One way to counter that tendency is to make the criteria for α-helices and β-strands stricter. We found that, by filtering PsiPred (http://bioinf.cs.ucl.ac.uk/psipred) (35) helix propensity scores (p_{Hlx}) with a very high cutoff of 0.99, the surviving helix predictions usually correspond well with residues identified by NMR as having high helix propensities. For example, for Mev-P_{NTD}, PsiPred plus filtering predicts residues 14-17, 28-33, and 191-193 as helical; all of them are in regions that form transient helices according to chemical shifts (26). Likewise long helices are also correctly predicted for Sev-NT (residues 477-489) and CBP-ID4 (residues 6-17 and 105-116).

We apply a boost factor, B_{Hlx}, to helices with a threshold length of 12:

$$B_{\mathrm{Hlx}} = 1 + \alpha p_{\mathrm{Hlx}} \Theta(p_{\mathrm{Hlx}} \geq 0.99; L_{\mathrm{Hlx}} \geq 12) \quad (3)$$

The Θ function is 1 if the helix propensity score is above the filtering cutoff and the helix length (L_{Hlx}) is above the threshold, and 0 otherwise. With a boost amplitude α at 0.5, the boosted SeqDYN prediction for Sev-NT reaches excellent agreement with the measured R_2 (Fig. 4E, red curve). The RMSE(-1) is reduced from 0.76 s^{-1} to 0.38 s^{-1} upon boosting. Applying the same helix boost to CBP-ID4 also results in a modest reduction in RMSE(-1), from 2.01 to 1.90 s^{-1} (Fig. 4F, red curve). The only other IDP for which PsiPred plus filtering predicts a long helix is the N-terminal region of lysyl-tRNA synthetase (KRS-NT). The authors who studied this protein did not report on secondary structure (36), but feeding their

reported chemical shifts to the TALOS+ server (https://spin.niddk.nih.gov/bax/nmrserver/talos/) (37) found only short stretches of residues that fall into the helical region of the Ramachandran map. The SeqDYN prediction for KRS-NT is already good [RMSE(-1) = 0.83 s^{-1}]; applying a helix boost would deteriorate the RMSE(-1) to 1.16 s^{-1}.

Further test on a set of nine IDPs

We have reserved nine IDPs for testing SeqDYN (parameterized on the training set of 45 IDPs). The level of disorder in these test proteins also spans the full range, from absence of secondary structures [ChiZ N-terminal region (12), Pdx1 C-terminal region (11), and TIA-1 prion-like domain (17)] to presence of transient short helices [synaptobrevin-2 (7), α-endosulfine (38), YAP (6), angiomotin-like 1 (AMOTL1) (39)] to formation of stable long helices [FtsQ (13) and CAHS-8 (9)]. For eight of the nine test IDPs, the RMSEs of SeqDYN predictions are lower than the experimental σ_{R_2} values, by an average of 0.62 s^{-1}. For the nineth IDP (Pdx1), the SeqDYN RMSE is slightly higher, by 0.06 s^{-1}, than the experimental σ_{R_2}.

The comparison of predicted and measured R_2 profiles along the sequence is presented in Fig. 5A-I. For ChiZ, SeqDYN correctly predicts the major peak around Arg25 and the minor peak around Arg46 (Fig. 5A). The R_2 profile of Pdx1 is largely featureless, except for a dip around Gly216, which is correctly predicted by SeqDYN (Fig. 5B). Correct prediction is also obtained for the higher R_2 in the first half of TIA-1 prion-like domain than in the second half (Fig. 5C). SeqDYN gives an excellent prediction for synaptobrevin-2, including a linear increase up to Arg56 and the major peak around Trp89 (Fig. 5D).

The prediction is also very good for α-endosulfine, including elevated R_2 around Glu34, which coincides with the presence of a transient helix, and depressed R_2 in the last 40 residues (Fig. 5E). The only miss is an underprediction for the peak around Lys74. SeqDYN also predicts well the overall shape of the R_2 profile for YAP, including peaks around Asn70,

Leu91, Arg124, and Arg161, but severely underestimates the peak height around Asn70 (Fig. 5F).NOE signals indicate contacts between Met86, Leu91, Fhe95, and Fhe96 (6); evidently this type of local contacts is captured well by SeqDYN. The R_2 elevation around Asn70 is mostly due to helix formation: residues 61-74 have helix propensities up to 40% (6). PsiPred predicts helix for residues 62-73, but only residues 65-68 survive the filtering that we impose, resulting a helix that is too short to apply a helix boost. The prediction for AMOTL1 is mostly satisfactory, including peaks around Phe200 and Arg264 and a significant dip around Gly292 (Fig. 5G). However, whereas the two peaks have approximately equal heights in the measured R_2 profile, the predicted peak height around Phe200 is too low. SCSs indicate helix propensity around both R_2 peaks (39). PsiPred also predicts helix in both regions, but only five and two residues, respectively, survive after filtering, which are too short for applying a helix boost.

For FtsQ, SeqDYN correctly predicts elevated R_2 for the long helix [residues 46-74 (13)] but underestimates the magnitude (RMSE = 2.32 s^{-1}; green curve in Fig. 5H). PsiPred plus filtering predicts a long helix formed by residues 47-73. Applying the helix boost substantially improves the agreement with the measured R_2, with RMSE reducing to 1.71 s^{-1} (red curve in Fig. 5H). SeqDYN also gives a qualitatively correct R_2 profile for CAHS-8, with higher R_2 for the middle section (residues 95-190) (RMSE = 2.36 s^{-1}; green curve in Fig. 5I). However, it misses the extra elevation in R_2 for the first half of the middle section (residues 95-145). According to SCS, the first and second halves have helix propensities of 60% and 30%, respectively (9). PsiPred plus filtering predicts helices for residues 96-121, 124-141, 169-173, and 179-189. Only the first two helices, both in the first half of the middle section, are considered long according to our threshold. Once again, applying the helix boost leads to marked improvement in the predicted in R_2, with RMSE reducing to 1.92 s^{-1} (red curve in Fig. 5I).

Inputting the sequence of a structured protein predicts R_2 in the unfolded state

SeqDYN is trained on IDPs, what if we feed it with the sequence of a structured protein? The prediction using the sequence of hen egg white lysozyme, a well-studied single-domain protein, is displayed in Fig. 6A. It shows remarkable agreement with the R_2 profile measured by Klein-Seetharaman et al. (3) in the unfolded state (denatured by 8 M urea and reduced to break disulfide bridges), including a major peak around Trp62, a second peak around Trp111, and a third peak around Trp123. Klein-Seetharaman et al. mutated Trp62 to Gly and the major peak all but disappeared. This result is also precisely predicted by SeqDYN with the mutant sequence (Fig. 6B).

Discussion

We have developed a powerful method, SeqDYN, that predicts the backbone amide transverse relaxation rates (R_2) of IDPs. The method is based on IDP sequences, is extremely fast, and available as a web server at https://zhougroup-uic.github.io/SeqDYNidp/. The excellent performance supports the notion that the ns-dynamics reported by R_2 is coded by the local sequence, comprising up to 6 residues on either side of a given residue. The amino-acid types that contribute the most to coupling within a local sequence are aromatic (Trp, Tyr, Phe, and His), Arg, and long branched aliphatic (Ile and Leu), suggesting the importance of π-π, cation-π, and hydrophobic interactions in raising R_2. These interactions are interrupted by Gly and amino acids with short polar sidechains (Ser, Thr, Asn, and Asp), leading to reduced R_2. Transient short helices produce moderate elevation in R_2, whereas stable long helices result in a big boost in R_2. Tertiary contacts can also raise R_2, but appears to be infrequent in most IDPs (1).

Our method incorporates ideas from a number of previous efforts at describing R_2. The first serious effort was by Schwalbe et al. (15), who accounted for contributions from neighboring residues as additive terms, instead of multiplicative factors as in SeqDYN. Cho et al. (16) and Delaforge et al. (24) used the running average of the bulkiness parameter over a window of five to nine residues as a qualitative indicator of R_2. Here again the calculation

was based on an additive model. Sekiyama et al. (17) employed a multiplicative model, with R_2 calculated as a geometric mean of "indices of local dynamics" over a five-residue window. These indices, akin to our q parameters, were trained on a single IDR (TIA-1 prion-like domain) and used to reproduce the measured R_2 for the same IDR. As we have illustrated on CBP-ID4 (Fig. S3), training on a single protein merely biases the parameters to that model and has little value in predicting R_2 for other proteins. In comparison, SeqDYN is trained on 45 IDPs and its predictions are robust and achieve quantitative agreement with measured R_2.

Ten of the IDPs tested here have been studied recently by MD simulations using IDP-specific force fields (1, 12-14). In Table 1 we compare the RMSEs of SeqDYN predictions with those for R_2 calculations from MD simulations. For five of these IDPs: A1-LCD, Aβ40, α-synuclein, tau K18, and FtsQ, RMSEs of SeqDYN and MD are remarkably similar. Four of these IDPs lack significant population of α-helices or β-sheets, but FtsQ forms a stable long helix. For one other IDP, namely HOX-DFD, MD, by explicitly modeling its folded domain, does a much better job in predicting R_2 than SeqDYN (RMSEs of 1.40 s^{-1} vs 1.99 s^{-1}). However, for the four remaining IDPs: p53TAD, Pup, Sev-NT, and ChiZ, SeqDYN significantly outperforms MD, with RMSEs averaging only 0.47 s^{-1}, compared to the MD counterpart of 1.14 s^{-1}. Overall, SeqDYN is very competitive against MD in predicting R_2, but without the significant computational cost. While MD simulations can reveal details of local interactions, as noted for α-synuclein, and capture tertiary interactions if they occur, they still suffer from perennial problems of force-field imperfection and inadequate sampling. SeqDYN provides an accurate description of IDP dynamics at a "mean-field" level, but could miss idiosyncratic behaviors of specific local sequences.

Deep-learning models have become very powerful, but they usually have millions of parameters and require millions of protein sequences for training (40). In contrast, SeqDYN employs a mathematical model with dozens of parameters and requires only dozens of proteins for training. Reduced models (by collapsing amino acids into a small number of distinct types) have even been trained on < 10 IDPs to predict propensities for binding

nanoparticles (18) or membranes (19). The mathematical model-based approach may be useful in other applications where data, similar to R_2, are limited, including predictions of IDP secondary chemical shifts or residues that bind drug molecules (41) or protein targets, or even in protein design, e.g., for recognizing an antigenic site or a specific DNA site.

Methods

Collection of IDPs with measured R_2

Starting from six nonhomologous IDPs in our previous MD study (1), we obtained R_2 data for eight IDPs from the Bimolecular Magnetic Resonance Data Bank (BMRB; https://bmrb.io); data for two other IDPs were from our collaborators (12, 13). Most of the 54 IDPs studied here were from searching the literature. Disorder was judged by dispersion in backbone amide proton chemical shifts, NOE, and SCS. R_2 data that were not available from the authors or BMRB were obtained by digitizing R_2 plots presented in figures of published papers, using WebPlotDigitizer (https://automeris.io/WebPlotDigitizer) (42) and further inspected visually.

Homology of IDPs was checked by sequence alignment using Clustal W (http://www.clustal.org/clustal2) (43), and presented as a clock-like tree using the "ape" package (http://ape-package.ird.fr) (44). IDPs that had discernible homology with the selected training set were removed. Removed IDPs included HOX-SCR and β-synuclein from our previous MD study (1), due to homology with HOX-DFD and α-synuclein, respectively.

Coding for SeqDYN

The training of SeqDYN was coded in python, similar to our previous work for predicting residue-specific membrane association propensities (ReSMAP; https://zhougroup-uic.github.io/ReSMAPidp/) (19). The cost function was the sum of mean-squared-errors for the IDPs in the training set. We used the least_squares function in scipy.optimize, with Trust Region Reflective as the minimization algorithm and all parameters restricted to the positive

range. For the web server (https://zhougroup-uic.github.io/SeqDYNidp/), we rewrote the prediction code javascript.

ACKNOWLEDGEMENTS

This work was supported by Grant GM118091 from the National Institutes of Health.

REFERENCES

1. S. Dey, M. MacAinsh, H. X. Zhou, Sequence-Dependent Backbone Dynamics of Intrinsically Disordered Proteins. *J Chem Theory Comput* **18**, 6310-6323 (2022).
2. A. R. Camacho-Zarco *et al.*, NMR Provides Unique Insight into the Functional Dynamics and Interactions of Intrinsically Disordered Proteins. *Chem Rev* **122**, 9331-9356 (2022).
3. J. Klein-Seetharaman *et al.*, Long-Range Interactions Within a Nonnative Protein. *Science* **295**, 1719-1722 (2002).
4. A. Abyzov *et al.*, Identification of Dynamic Modes in an Intrinsically Disordered Protein Using Temperature-Dependent NMR Relaxation. *J Am Chem Soc* **138**, 6240-6251 (2016).
5. R. Schneider *et al.*, Visualizing the Molecular Recognition Trajectory of an Intrinsically Disordered Protein Using Multinuclear Relaxation Dispersion NMR. *J Am Chem Soc* **137**, 1220-1229 (2015).
6. M. Feichtinger *et al.*, Long-range structural preformation in yes-associated protein precedes encounter complex formation with TEAD. *iScience* **25**, 104099 (2022).
7. N.-A. Lakomek, H. Yavuz, R. Jahn, Á. Pérez-Lara, Structural dynamics and transient lipid binding of synaptobrevin-2 tune SNARE assembly and membrane fusion. *Proc Natl Acad Sci U S A* **116**, 8699-8708 (2019).

8. A. E. Conicella, G. H. Zerze, J. Mittal, N. L. Fawzi, ALS Mutations Disrupt Phase Separation Mediated by alpha-Helical Structure in the TDP-43 Low-Complexity C-Terminal Domain. *Structure* **24**, 1537-1549 (2016).

9. A. Malki *et al.*, Intrinsically Disordered Tardigrade Proteins Self-Assemble into Fibrous Gels in Response to Environmental Stress. *Angew Chem Int Ed Engl* **61**, e202109961 (2022).

10. E. W. Martin *et al.*, Valence and patterning of aromatic residues determine the phase behavior of prion-like domains. *Science* **367**, 694-699 (2020).

11. E. C. Cook, D. Sahu, M. Bastidas, S. A. Showalter, Solution Ensemble of the C-Terminal Domain from the Transcription Factor Pdx1 Resembles an Excluded Volume Polymer. *J Phys Chem B* **123**, 106-116 (2019).

12. A. Hicks, C. A. Escobar, T. A. Cross, H. X. Zhou, Sequence-dependent correlated segments in the intrinsically disordered region of ChiZ. *Biomolecules* **10**, 1-23 (2020).

13. S. T. Smrt, C. A. Escobar, S. Dey, T. A. Cross, H. X. Zhou, An Arg / Ala-Rich Helix in the N-Terminal Region of M . tuberculosis FtsQ Anchors FtsZ to Membranes. *biorxiv*, DOI: 10.1101/2022.1109.1102.506397v506392 (2022).

14. L. Yu, R. Bruschweiler, Quantitative prediction of ensemble dynamics, shapes and contact propensities of intrinsically disordered proteins. *PLoS Comput Biol* **18**, e1010036 (2022).

15. H. Schwalbe *et al.*, Structural and dynamical properties of a denatured protein. Heteronuclear 3D NMR experiments and theoretical simulations of lysozyme in 8 M urea. *Biochemistry* **36**, 8977-8991 (1997).

16. M. K. Cho *et al.*, Amino acid bulkiness defines the local conformations and dynamics of natively unfolded alpha-synuclein and tau. *J Am Chem Soc* **129**, 3032-3033 (2007).

17. N. Sekiyama *et al.*, ALS mutations in the TIA-1 prion-like domain trigger highly condensed pathogenic structures. *Proc Natl Acad Sci U S A* **119**, e2122523119 (2022).

18. D. W. Li, M. Xie, R. Bruschweiler, Quantitative cooperative binding model for intrinsically disordered proteins interacting with nanomaterials. *J Am Chem Soc* **142**, 10730-10738 (2020).

19. S. Qin, A. Hicks, S. Dey, R. Prasad, H. X. Zhou, ReSMAP: Web Server for Predicting Residue-Specific Membrane-Association Propensities of Intrinsically Disordered Proteins. *Membranes* **12**, 773 (2022).

20. M. R. Jensen *et al.*, Quantitative conformational analysis of partially folded proteins from residual dipolar couplings: application to the molecular recognition element of Sendai virus nucleoprotein. *J Am Chem Soc* **130**, 8055-8061 (2008).

21. A. Piai *et al.*, Just a Flexible Linker? The Structural and Dynamic Properties of CBP-ID4 Revealed by NMR Spectroscopy. *Biophys J* **110**, 372-381 (2016).

22. S. Maiti *et al.*, Dynamic Studies on Intrinsically Disordered Regions of Two Paralogous Transcription Factors Reveal Rigid Segments with Important Biological Functions. *J Mol Biol* **431**, 1353-1369 (2019).

23. S. Patel, V. Ramanujam, A. K. Srivastava, K. V. Chary, Conformational propensities and dynamics of a betagamma-crystallin, an intrinsically disordered protein. *Phys Chem Chem Phys* **16**, 12703-12718 (2014).

24. E. Delaforge *et al.*, Deciphering the Dynamic Interaction Profile of an Intrinsically Disordered Protein by NMR Exchange Spectroscopy. *J Am Chem Soc* **140**, 1148-1158 (2018).

25. Y. H. Sung, D. Eliezer, Residual structure, backbone dynamics, and interactions within the synuclein family. *J Mol Biol* **372**, 689-707 (2007).

26. S. Milles *et al.*, An ultraweak interaction in the intrinsically disordered replication machinery is essential for measles virus function. *Sci Adv* **4**, eaat7778 (2018).

27. Z. Sólyom *et al.*, The Disordered Region of the HCV Protein NS5A: Conformational Dynamics, SH3 Binding, and Phosphorylation. *Biophys J* **109**, 1483-1496 (2015).

28. E. W. Martin *et al.*, Sequence Determinants of the Conformational Properties of an Intrinsically Disordered Protein Prior to and upon Multisite Phosphorylation. *J Am Chem Soc* **138**, 15323-15335 (2016).

29. A. M. Janke *et al.*, Lysines in the RNA Polymerase II C-Terminal Domain Contribute to TAF15 Fibril Recruitment. *Biochemistry* **57**, 2549-2563 (2018).

30. M. Jenner *et al.*, Mechanism of intersubunit ketosynthase–dehydratase interaction in polyketide synthases. *Nat Chem Biol* **14**, 270-275 (2018).

31. E. M. Bafaro, M. W. Maciejewski, J. C. Hoch, R. E. Dempski, Concomitant disorder and high-affinity zinc binding in the human zinc- and iron-regulated transport protein 4 intracellular loop. *Protein Sci* **28**, 868-880 (2019).

32. M. G. Murrali, A. Piai, W. Bermel, I. C. Felli, R. Pierattelli, Proline Fingerprint in Intrinsically Disordered Proteins. *ChemBioChem* **19**, 1625-1629 (2018).

33. L. E. Wong, T. H. Kim, D. R. Muhandiram, J. D. Forman-Kay, L. E. Kay, NMR Experiments for Studies of Dilute and Condensed Protein Phases: Application to the Phase-Separating Protein CAPRIN1. *J Am Chem Soc* **142**, 2471-2489 (2020).

34. J. M. Zimmerman, N. Eliezer, R. Simha, The characterization of amino acid sequences in proteins by statistical methods. *J Theor Biol* **21**, 170-201 (1968).

35. L. J. McGuffin, K. Bryson, D. T. Jones, The PSIPRED protein structure prediction server. *Bioinformatics* **16**, 404-405 (2000).

36. H. Y. Cho *et al.*, Characterization of the interaction between lysyl-tRNA synthetase and laminin receptor by NMR. *FEBS Lett* **588**, 2851-2858 (2014).

37. Y. Shen, F. Delaglio, G. Cornilescu, A. Bax, TALOS+: a hybrid method for predicting protein backbone torsion angles from NMR chemical shifts. *J Biomol NMR* **44**, 213-223 (2009).

38. C. Thapa, P. Roivas, T. Haataja, P. Permi, U. Pentikainen, Interaction mechanism of endogenous PP2A inhibitor protein ENSA with PP2A. *FEBS J* **289**, 519-534 (2022).

39. A. Vogel, A. Crawford, A. Nyarko, Multivalent Angiomotin-like 1 and Yes-associated protein form a dynamic complex. *Protein Sci* **31**, e4295 (2022).

40. A. Rives *et al.*, Biological structure and function emerge from scaling unsupervised learning to 250 million protein sequences. *Proc Natl Acad Sci U S A* **118**, e2016239118 (2021).

41. P. Robustelli *et al.*, Molecular Basis of Small-Molecule Binding to alpha-Synuclein. *J Am Chem Soc* **144**, 2501-2510 (2022).

42. A. Rohatgi, *Webplotdigitizer: Version 4.6* (2022).

43. M. A. Larkin *et al.*, Clustal W and Clustal X version 2.0. *Bioinformatics* **23**, 2947-2948 (2007).

44. E. Paradis, J. Claude, K. Strimmer, APE: Analyses of Phylogenetics and Evolution in R language. *Bioinformatics* **20**, 289-290 (2004).

45. A. Hicks, M. MacAinsh, H. X. Zhou, Removing thermostat distortions of protein dynamics in constant-temperature molecular dynamics simulations. *J Chem Theory Comput* **17**, 5920-5932 (2021).

46. H. J. Feldman, C. W. Hogue, Probabilistic sampling of protein conformations: new hope for brute force? *Proteins* **46**, 8-23 (2002).

47. P. Bernado, M. Blackledge, A self-consistent description of the conformational behavior of chemically denatured proteins from NMR and small angle scattering. *Biophys J* **97**, 2839-2845 (2009).

Table 1. RMSEs (s^{-1}) of R_2 predictions by SeqDYN and MD for 10 IDPs

IDP name	SeqDYN	MD
A1-LCD	0.60[a]	0.59[d, e]
Aβ40	0.38[a]	0.38[d]
HOX-DFD	1.99[a]	1.40[d]
α-synuclein	0.44[a]	0.50[d]
p53TAD	0.33[a]	1.04[f]
Pup	0.43[a]	1.00[f]
Sev-NT	0.38[a, b]	1.10[d, g]
tau K18	0.83[a]	0.80[d]
ChiZ	0.74[c]	1.40[h]
FtsQ	1.71[c, b]	1.70[i]

[a]Based on leave-one-out training (using 44 IDPs).

[b]Helix boost applied.

[c]Based on training by the full training set (45 IDPs).

[d]From ref (1).

[e]RMSE is scaled down by a factor of 2.39, to correct for the effect of temperature (MD at 288 K; see Fig. S2C).

[f]From ref (14).

[g]RMSE is scaled down by a factor of 2.99, to correct for the effects of temperature and magnetic field (MD at 274 K and 850 MHz; see Fig. S2B).

[h]Originally calculated in ref (12) with correction in ref (45).

[i]From ref (13).

FIGURE CAPTIONS

Figure 1. Representative conformations of five IDPs. (A-E) MKK4, α-synuclein, Mev-P_{NTD}, Sev-NT, and CBP-ID4. Conformations were initially generated using TraDES (http://trades.blueprint.org) (46), selected to have radius of gyration close to predicted by a scaling function $R_g = 2.54N^{0.522}$ (Å) (47). Conformations for residues predicted as helical by PsiPred plus filtering were replaced by ideal helix. Finally residues are colored according to a scheme ranging from green for low predicted R_2 to red for high predicted R_2.

Figure 2. Properties of the 45 IDPs in the training set. (A) Histograms of means and standard deviations, calculated for individual proteins. Curves are drawn to guide the eye. Inset: correlation between $\bar{R}_2$ and σ_{R_2}. (B) Experimental mean scaled R_2 (msR_2) and SeqDYN q parameters, for the 20 types of amino acids. Note that Pro residues have low msR_2 for the lack of backbone amide proton. Amino acids are in descending order of q.

Figure 3. SeqDYN model parameters. (A) Correlation between msR_2 and q. The values are also displayed as bars in Fig. 2B. (B) Correlation of msR_2 and q with amino-acid molecular mass. (C) Correlation of msR_2 and q with bulkiness. (D) The optimal correlation length and deterioration of SeqDYN prediction as the correlation length is moved away from the optimal value.

Figure 4. Quality of SeqDYN predictions. (A) Histogram of RMSE(-1). Letters indicate RMSE(-1) values of the IDPs to be presented in panels (B-F). (B-F) Measured (bars) and predicted (curves) R_2 profiles for MKK4, α-synuclein, Mev-P_{NTD}, Sev-NT, and CBP-ID4. In (E) and (F), green curves are SeqDYN predictions and red curves are obtained after a helix boost.

Figure 5. Measured (bars) and predicted (curves) R_2 profiles for ChiZ N-terminal region, TIA1 prion-like domain, Pdx1 C-terminal region, synaptobrevin-2, α-endosulfine, YAP, AMOTL1, FtsQ, and CAHS-8. In (C), R_2 does not fall off at the N-terminus because the sequence is preceded by an expression tag MGSSHHHHHHHHHHHS. In (H) and (I), green curves are SeqDYN predictions and red curves are obtained after a helix boost.

Figure 6. Predicted R_2 profiles (curves) for the lysozyme sequence and a mutant show close agreement with those measured (bars) on the proteins in the unfolded state. (A) Wild type. (B) With Trp62 to Gly mutation.

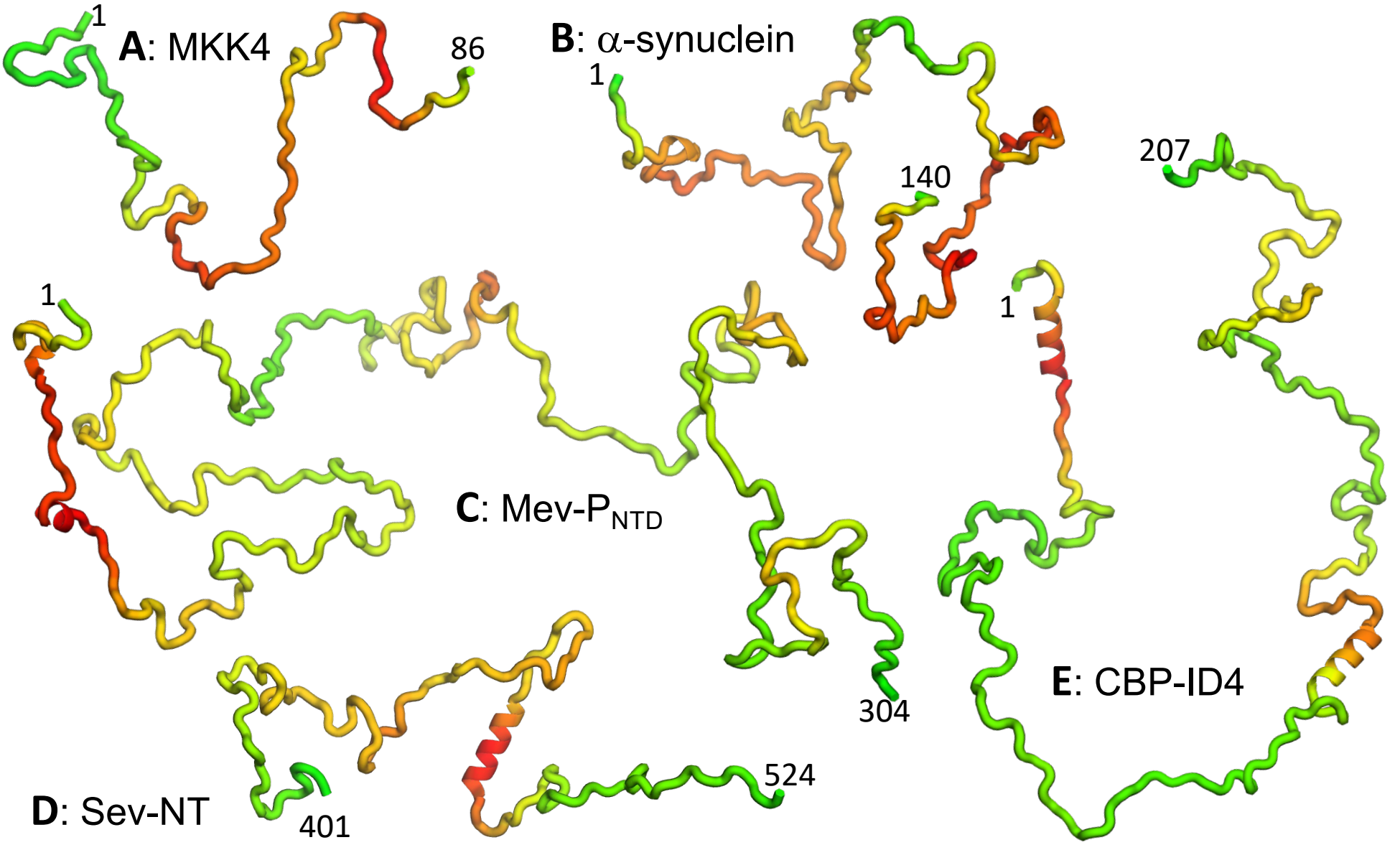
1
A: MKK4
86
B: α-synuclein
1
140
207
1
C: Mev-P$_{NTD}$
1
304
E: CBP-ID4
524
D: Sev-NT
401

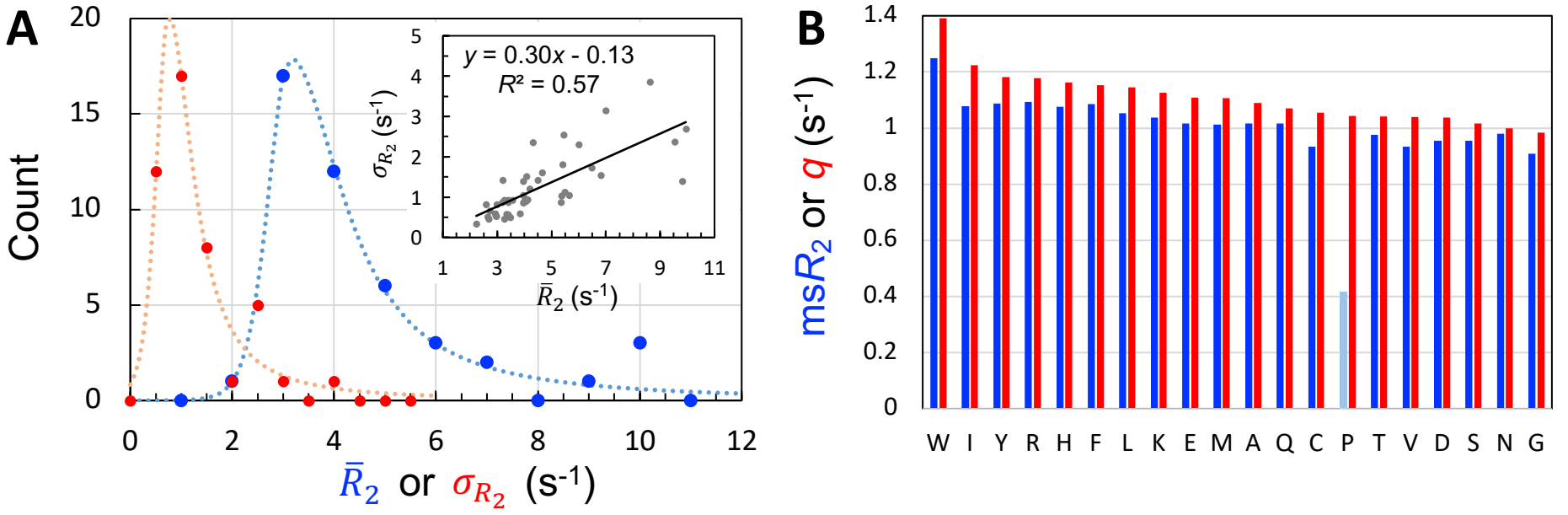
A
Count
20
15
10
5
0
0
2
4
6
8
10
12
$\bar{R}_2$ or σ_{R_2} (s^{-1})
y = 0.30x - 0.13
R² = 0.57
σ_{R_2} (s^{-1})
$\bar{R}_2$ (s^{-1})
B
msR$_2$ or q (s^{-1})
1.4
1.2
1
0.8
0.6
0.4
0.2
0
W I Y R H F L K E M A Q C P T V D S N G

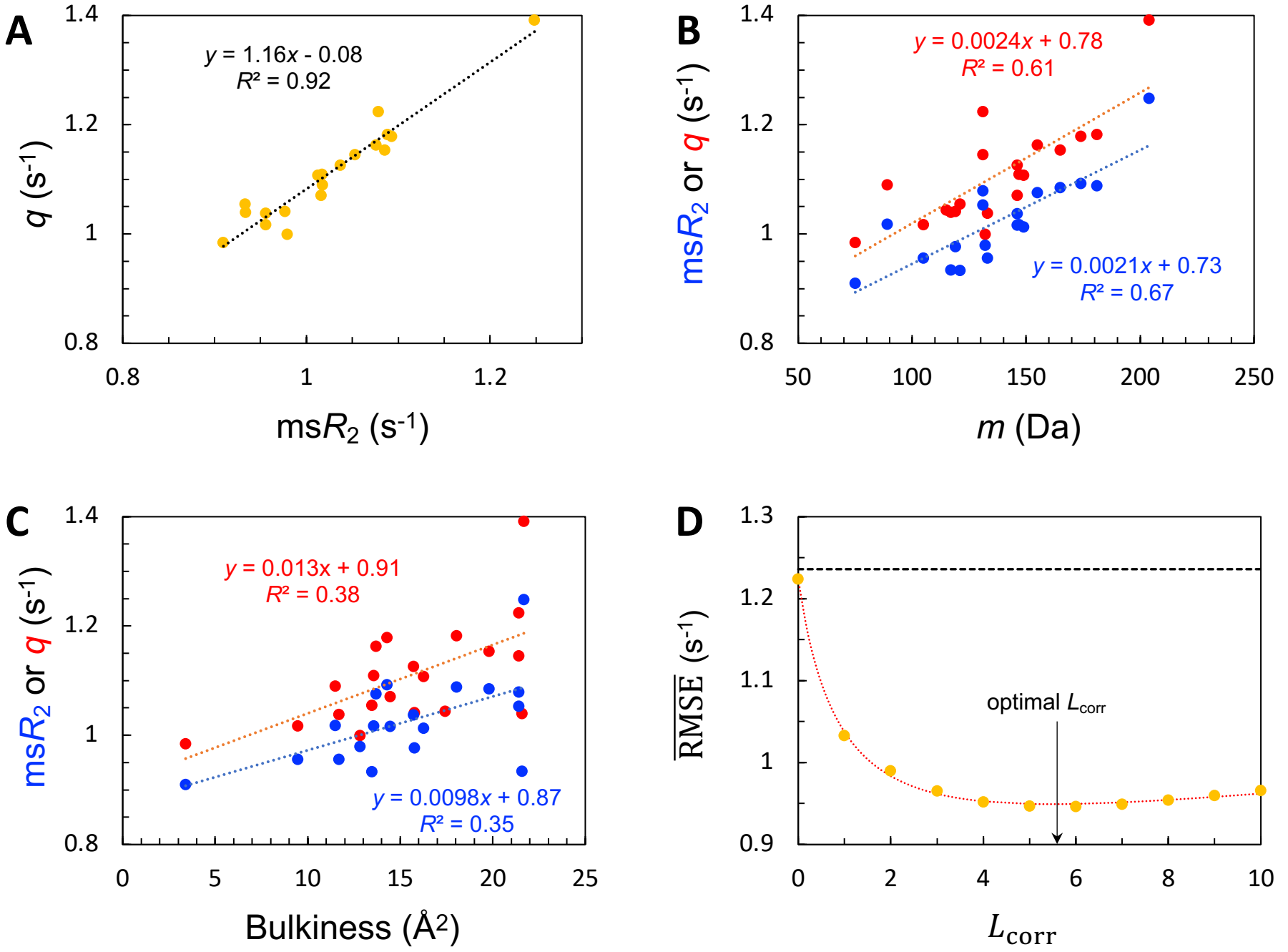
A
y = 1.16x - 0.08
R² = 0.92
q (s-1)
msR2 (s-1)
B
y = 0.0024x + 0.78
R² = 0.61
y = 0.0021x + 0.73
R² = 0.67
msR2 or q (s-1)
m (Da)
C
y = 0.013x + 0.91
R² = 0.38
y = 0.0098x + 0.87
R² = 0.35
msR2 or q (s-1)
Bulkiness (Å2)
D
optimal Lcorr
RMSE (s-1)
Lcorr

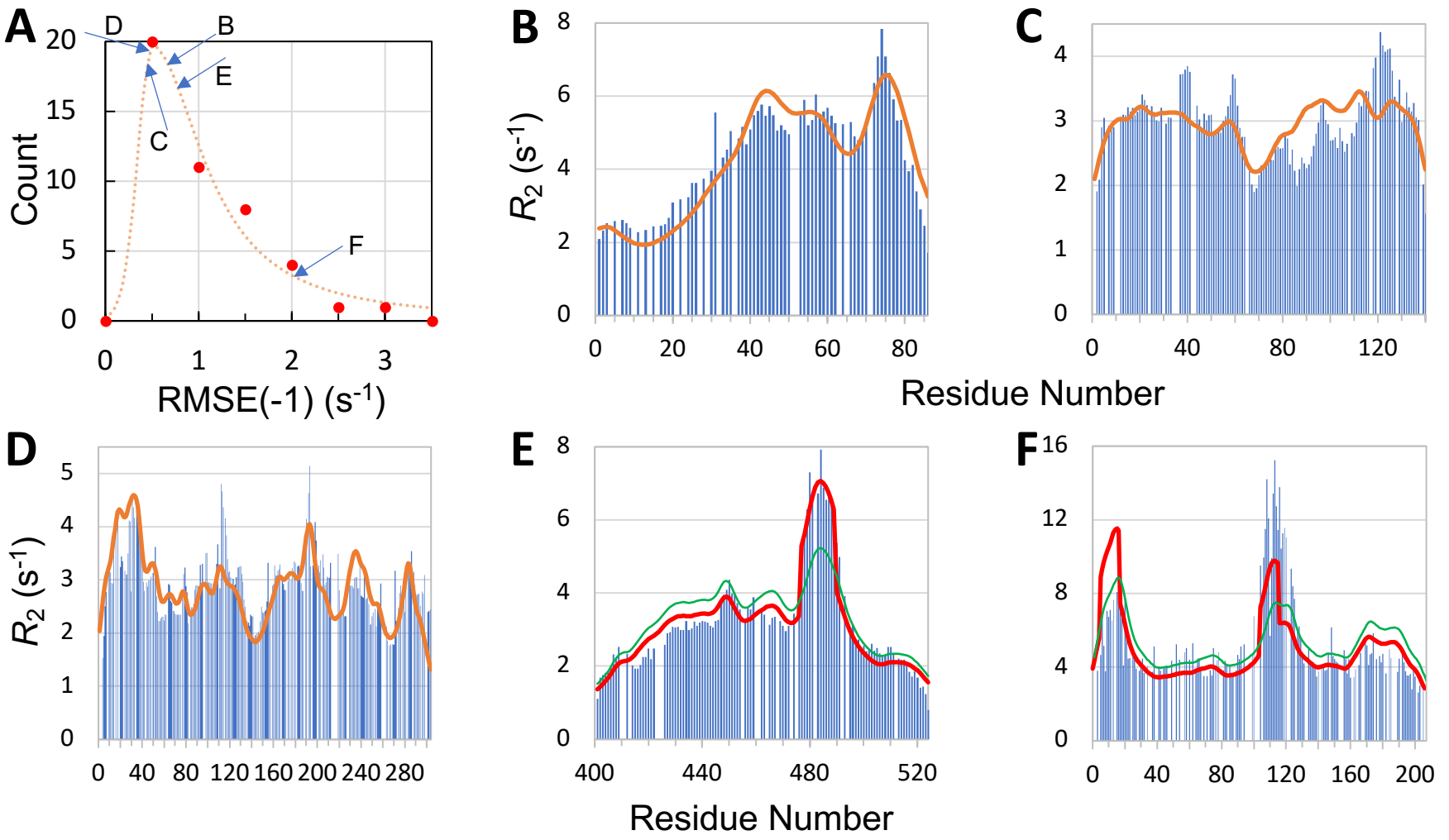
A
B
C
D
E
F
Count
RMSE(-1) (s-1)
R2 (s-1)
Residue Number

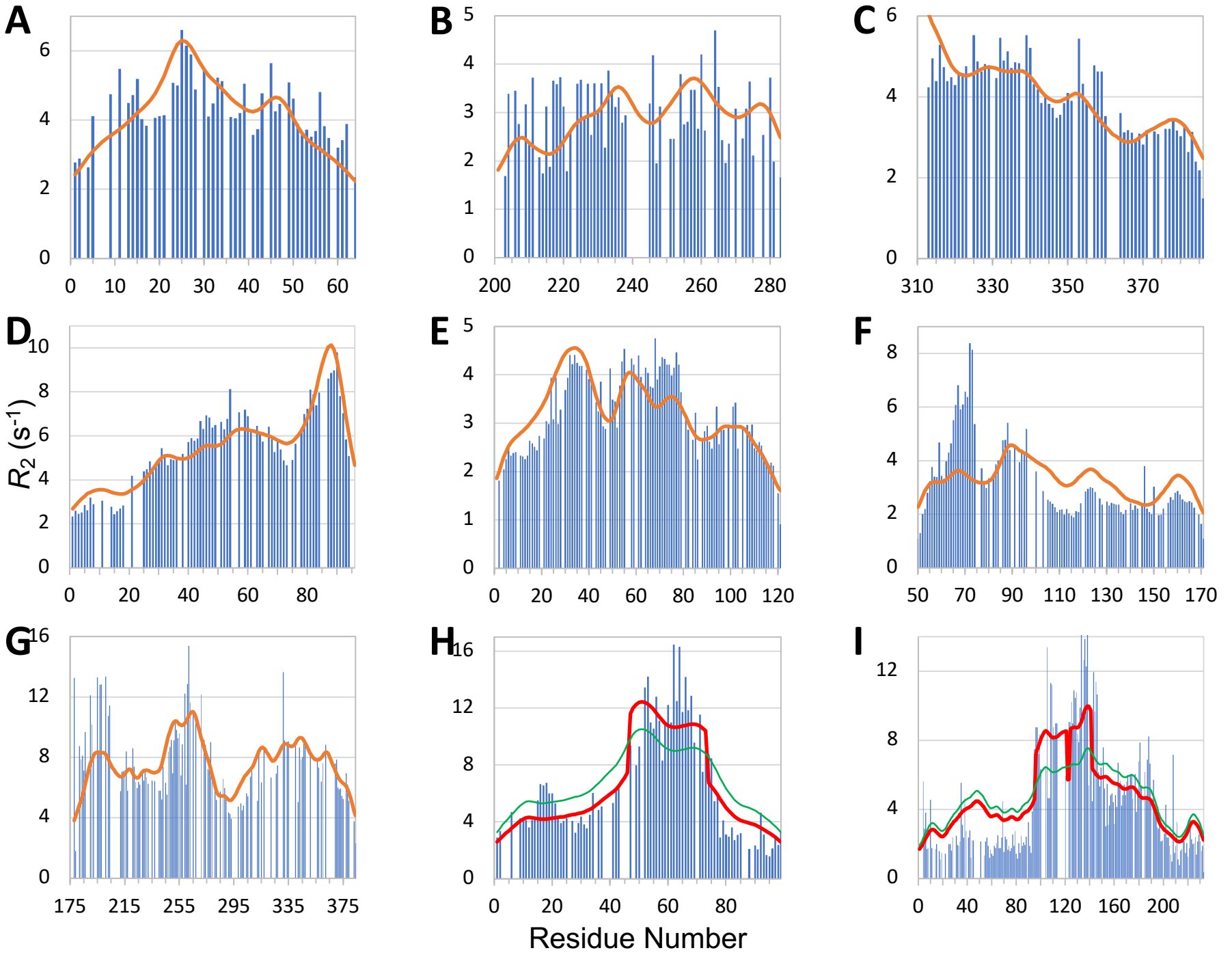
A
B
C
D
E
F
G
H
I
R_2 (s^{-1})
Residue Number

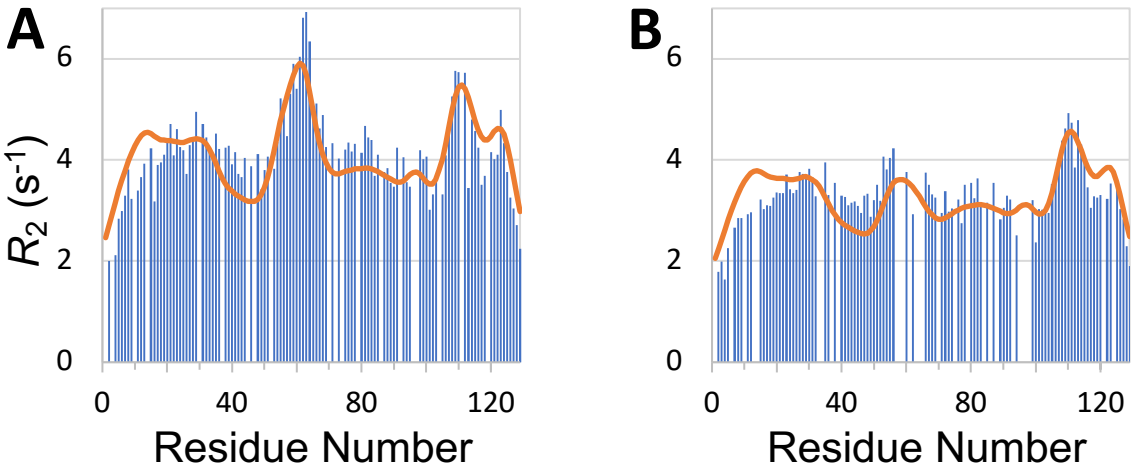
A
B
R_2 (s^{-1})
0
2
4
6
0
40
80
120
Residue Number
Residue Number

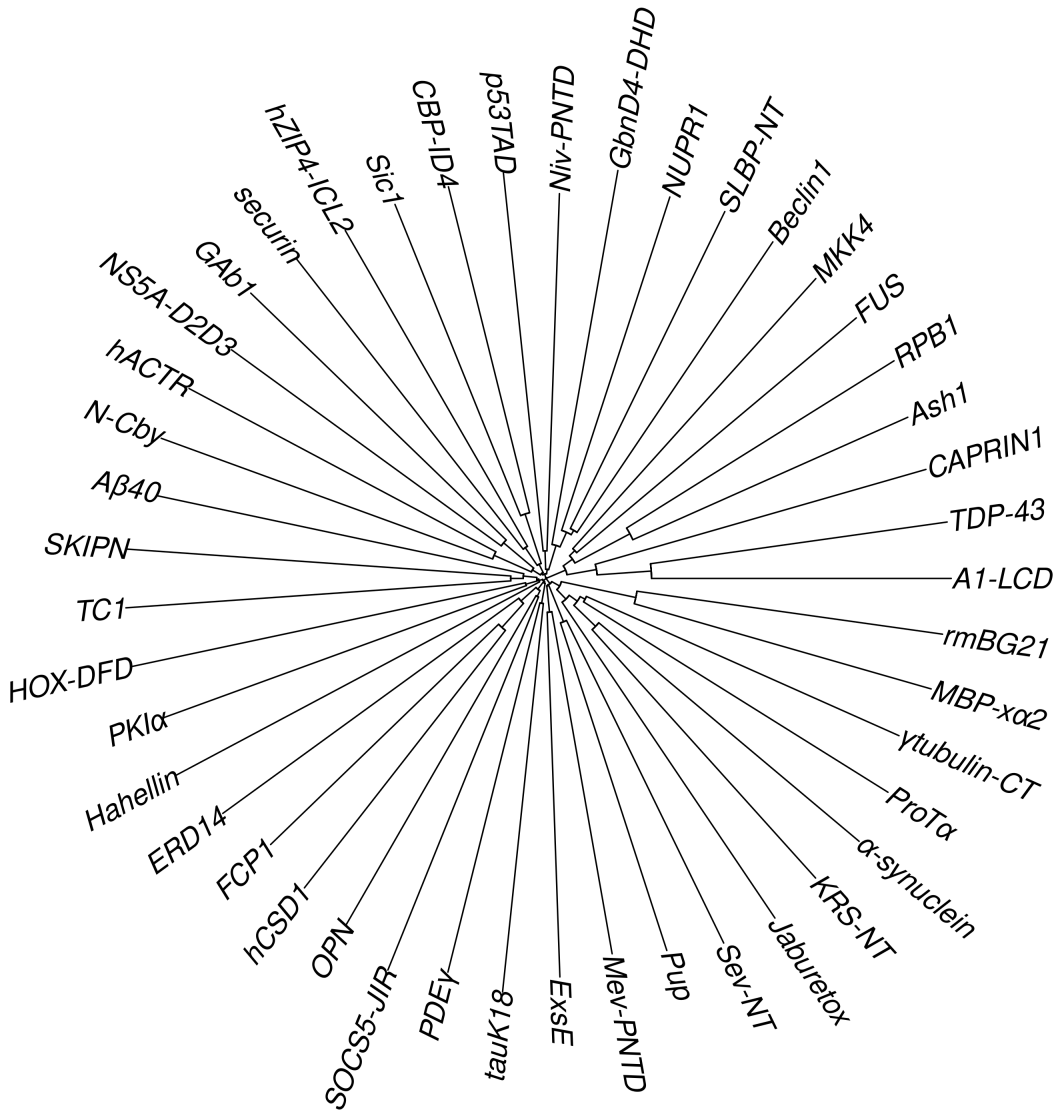
p53TAD
Niv-PNTD
GbnD4-DHD
NUPR1
SLBP-NT
Beclin1
MKK4
FUS
RPB1
Ash1
CAPRIN1
TDP-43
A1-LCD
rmBG21
MBP-xα2
γtubulin-CT
ProTα
α-synuclein
KRS-NT
Jaburetox
Sev-NT
Pup
Mev-PNTD
ExsE
8γκγnat
PDEγ
SOCS5-JIR
OPN
hCSD1
FCP1
ERD14
Hahellin
PKIα
HOX-DFD
TC1
SKIPN
Aβ40
N-Cby
hACTR
NS5A-D2D3
GAb1
securin
hZIP4-ICL2
Sic1
CBP-ID4

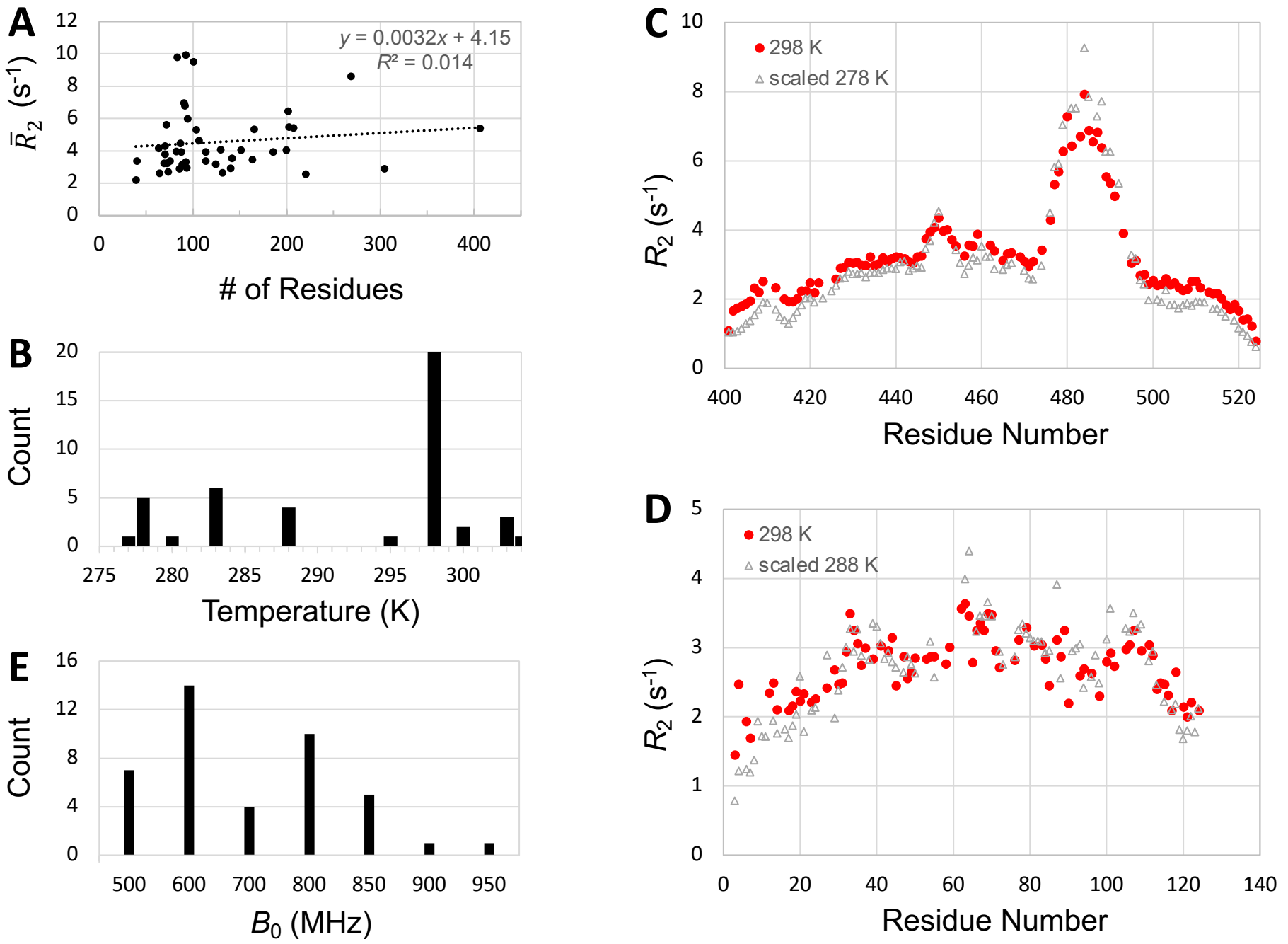
A
$\bar{R}_2$ (s^{-1})
y = 0.0032x + 4.15
R² = 0.014
# of Residues
B
Count
Temperature (K)
C
298 K
scaled 278 K
R_2 (s^{-1})
Residue Number
D
298 K
scaled 288 K
R_2 (s^{-1})
Residue Number
E
Count
B_0 (MHz)

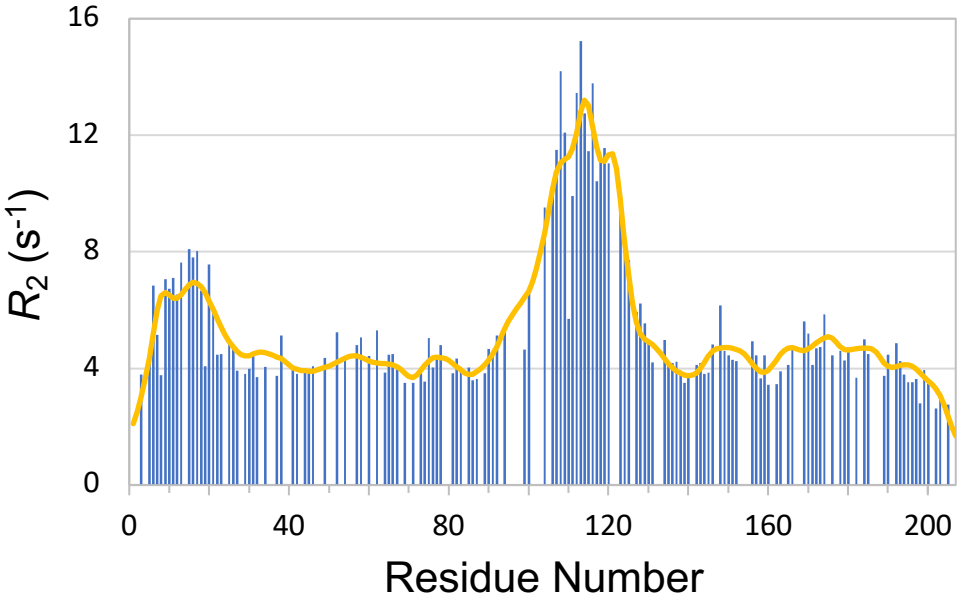
16
12
8
4
0
R_2 (s^{-1})
0
40
80
120
160
200
Residue Number